Morphology Development for Three-Component Emulsion Polymers: Theory and Experiments

ERIC J. SUNDBERG and DONALD C. SUNDBERG*

Polymer Research Group, Department of Chemical Engineering, University of New Hampshire, Durham, New Hampshire 03824

SYNOPSIS

Three-component emulsion polymer systems constitute an overall four-component system from a morphological viewpoint. The aqueous phase is always the continuous phase within which 22 distinct and thermodynamically stable particle morphologies may exist. Six uniquely different categories of particles compose this morphological menu and may be identified as core–shell–shell, hemicore, hemishell, trisectional, "snowman," and cored hemisphere. Extension of previously published free-energy thermodynamic analyses of two component emulsion polymers has resulted in the ability to predict the most likely equilibrium morphology to be found for three-component particles. Predictions have been carried out for each possible three-component combination of poly(methyl methacrylate), polystyrene, poly(dimethyl siloxane), and polycarbonate. The results show that in nearly every instance two or three different morphologies are computed to possess nearly equivalent free energies, whereas all other possibilities would result in much higher free energies. This indicates that more precise knowledge of all interfacial tensions is required when considering three-component systems than was found to be generally needed for two-component systems. Experiments were carried out for each polymer combination using a very surface-active emulsifier (sodium lauryl sulfate) and, separately, a weakly surface-active emulsifier (natural pectin). For this choice of polymers and emulsifiers, only three of the six unique morphological categories were found experimentally. In all cases, the thermodynamic analysis predicted the experimentally determined morphology to possess the lowest or next to lowest free energy. © 1993 John Wiley & Sons, Inc.

INTRODUCTION

Emulsion polymers are important items of commerce, finding application in a wide variety of products that derive their properties from both the chemical and morphological characteristics of the latex. The morphological control of two-component polymer particles has recently received a significant level of attention in the literature.[1–16]. These reports have concentrated on the effects of the materials used in the latex formulation and upon the process used to produce the final latex. Of particular note is the critical role played by the interfacial tensions between the individual polymer phases and between the aqueous and polymer phases, particularly the latter.

Recently, advances in bulk-phase polymer blends have also recognized the role of interfacial tensions between the polymer phases. Hobbs and co-workers[17] described some morphological results of three-component blends and made use of spreading coefficients to serve as a guide to interpreting these morphologies. Their work showed that the two polymer components representing the minority-phase volumes would be distributed throughout a matrix phase in a variety of different forms, depending upon the interfacial tensions between the three component pairs of polymers. In a similar sense, we have investigated the morphological nature of three-component emulsion polymers. In such cases, one needs to consider the presence of water (containing a surfactant) in addition to the polymer

* To whom correspondence should be addressed.

Journal of Applied Polymer Science, Vol. 47, 1277–1294 (1993)
 CCC 0021-8995/93/071277-18

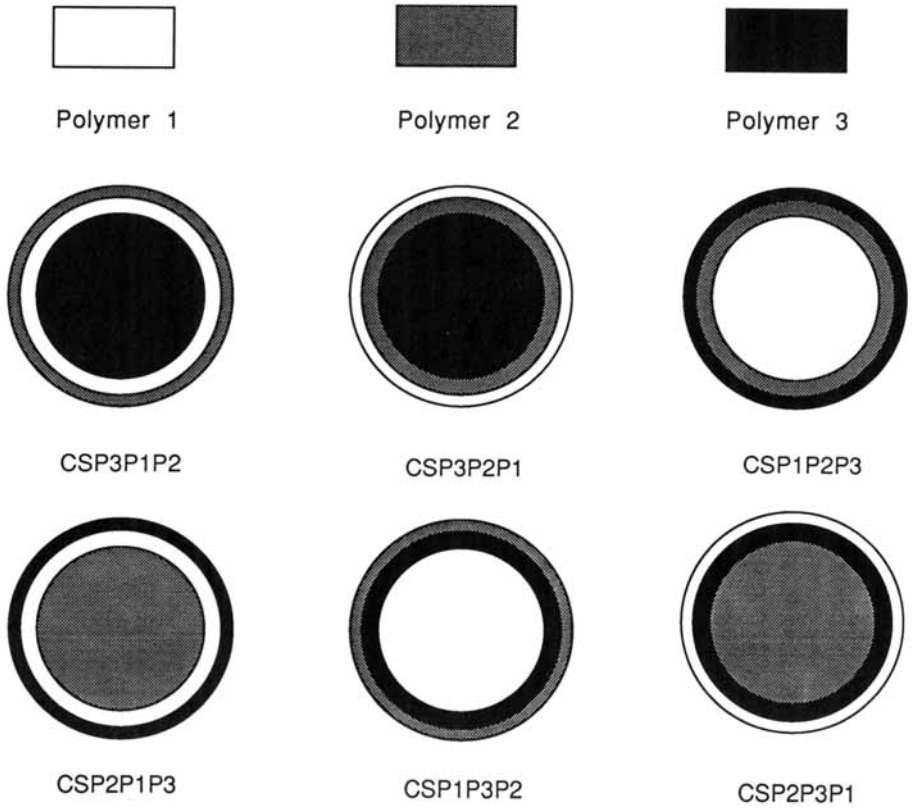

Figure 1 Core–shell–shell morphologies for three-component latex particles.

phases and take into account the interfacial tensions at the aqueous/polymer surfaces. Thus, when three-component emulsion polymers are in a latex form, one needs to consider a four-component system while investigating the possible particle structures; the aqueous phase is always the continuous phase. The goal of this work has been to identify the types of three-component particles that represent thermodynamically stable morphologies and to extend our previous quantitative treatment for two-component particles[12,18,19] in order to make predictions of three-component systems.

THERMODYNAMIC CONSIDERATIONS AND MORPHOLOGICAL ALTERNATIVES

Recent considerations of two-component latex particles have shown that only core–shell, inverted core–shell, and hemispherical particles are stable in a thermodynamic sense, although many other morphologies have been reported (including sandwiches, "confetti"-shaped particles, and occluded structures). When we consider three polymeric components within latex particles, a much greater number of stable morphological arrangements are possible. We have identified six uniquely different categories of such particles and distinguish them as core–shell–shell, hemicore, hemishell, trisectional, snowman, and cored hemisphere. These are shown in Figures 1–5 where we identify six each of the core–shell–shell and cored hemisphere alternatives, three each of the hemicore, hemishell, and snowman alternatives, and one trisectional alternative. Thus, by adding a third component to the simplest composite emulsion polymer system, one moves from the consideration of three to 22 morphological alternatives.

Rather than attempting to apply the spreading coefficient approach to these systems, we have chosen the more general approach of describing the free energy of the various morphological alternatives and determining that structure which contains the minimum free energy. Here, it is straightforward to make computations as a function of the relative volume fractions of the three polymers. In the following analysis, we compute the change in the Gibbs' free energy along the pathway shown in Figure 6, which assumes a starting point of a latex particle suspended in an aqueous phase and bulk phases of the other two polymers. The final state is that of one of the

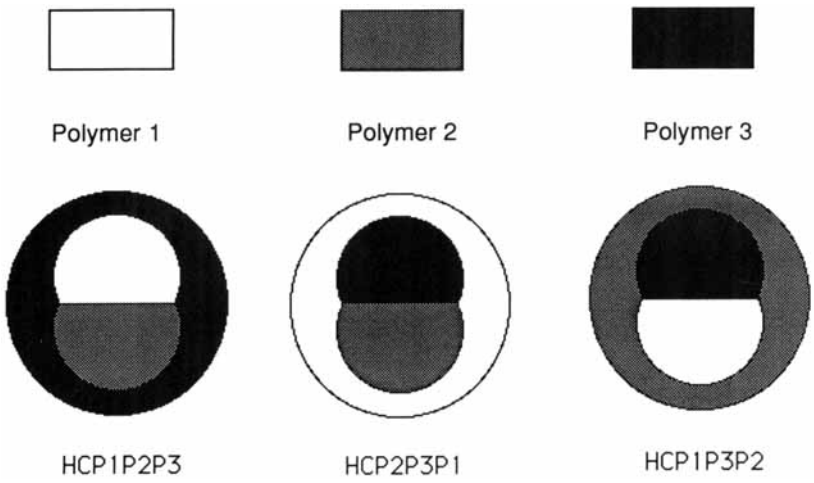

Figure 2 Hemicore morphologies for three-component latex particles.

22 possible equilibrium morphologies. The assignment of polymer components 1, 2, and 3 in Figure 6 is completely arbitrary and will not influence the free-energy analysis. This approach is consistent with that which we described in an earlier paper involving two-component particles.[12] As such, for any particular final morphological state,

$$\Delta G = \sum \gamma_i A_i - \gamma_0 A_0 \qquad (1)$$

where A_i is any interfacial area; γ_i, its corresponding interfacial tension; A_0, the interfacial area of the initial latex particle, and γ_0, its interfacial tension against the aqueous phase (containing surfactant). Since we apply eq. (1) to any of the morphological structures in Figures 1–5 and only at the end of the experiment where there is only pure polymer (no residual monomer or solvent), the enthalpic and entropic changes are the same for all structures and are thus excluded from further considerations. The application of eq. (1) requires only that the interfacial areas can be described and that the attendant interfacial tensions are known. It is true, of course, that the utility of eq. (1) will be restricted to situations where the particle morphology has developed slowly enough so that equilibrium conditions have applied throughout its development.

It is useful to modify eq. (1) by dividing through by A_0 and thus achieve a free-energy expression that is independent of particle size. Since its units are now those of interfacial tension, we write the reduced free-energy change as[12]

$$\Delta\gamma = \sum \gamma_i A_i / A_0 - \gamma_0 \qquad (2)$$

The $\Delta\gamma$ values so calculated will depend upon the particular choice of which polymeric constituents are designated to be components 1, 2, or 3 in Figure

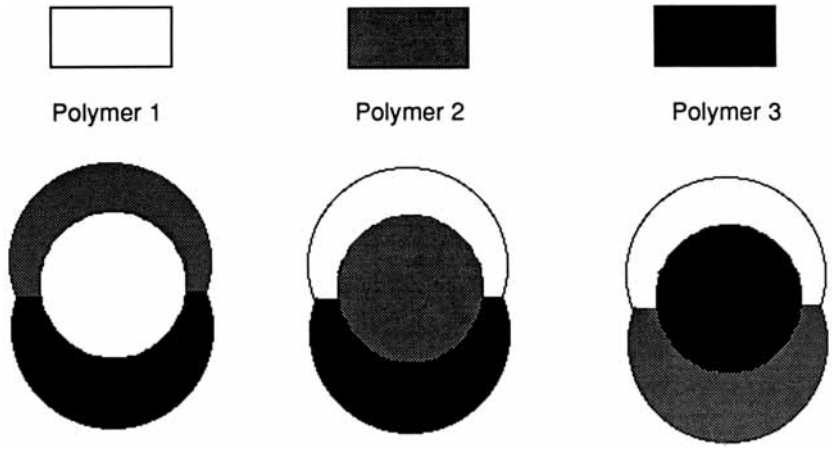

Figure 3 Hemishell morphologies for three-component latex particles.

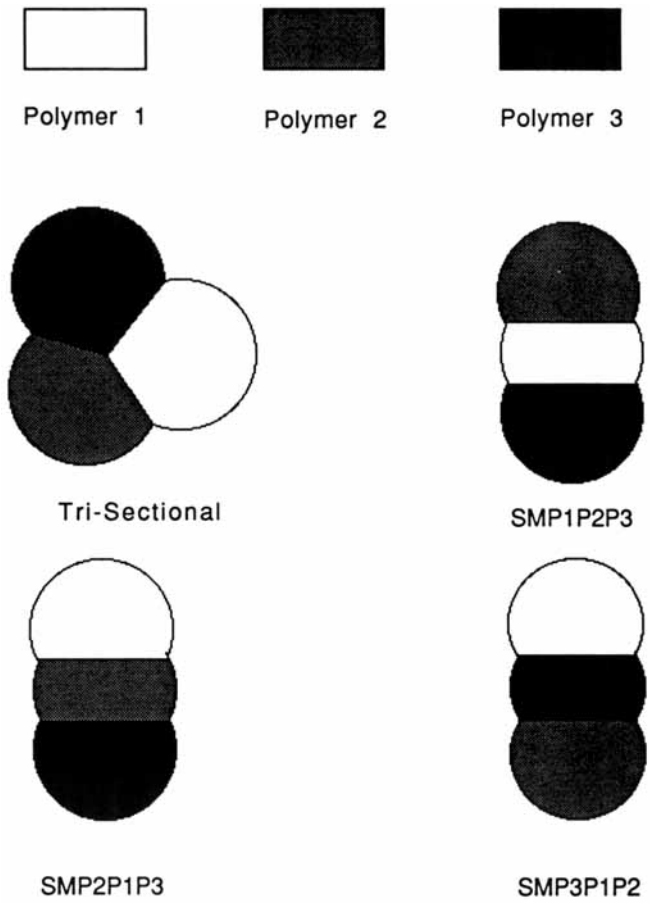

Figure 4 Trisectional and "snowman" morphologies for three-component latex particles.

6, as that choice will influence the value of γ_0 in eq. (2). However, since γ_0 is a constant, the determination of the morphological structure that represents the lowest free-energy state will be unaffected. Thus, we choose to retain the γ_0 term as we have in previous analyses.[12]

Some further nomenclature is useful as we consider applying eq. (2) to any of the 22 possible morphologies. Here, we utilize the nomenclature identified in Figures 1–5 to describe the various $\Delta\gamma$'s, and introduce symbols such as $(\Delta\gamma)_{CSP3P1P2}$ to depict the calculation for a core–shell–shell particle having polymer 3 as the core, polymer 1 as the inner shell, and polymer 2 as the outer shell. The interfaces that are important in this case are those between polymer 1 and polymer 3, γ_{P1P3}; polymer 1 and polymer 2, γ_{P1P2}; and polymer 2 and water (containing surfactant), γ_{P2W}. In all cases, γ_0 is written as γ_{P1W}.

For the case of the CSP3P1P2 particle shown in Figure 1, eq. (2) can be written as

$$(\Delta\gamma)_{CSP3P1P2} = \gamma_{P1P3}(R''_P/R_0)^2 + \gamma_{P1P2}(R'_P/R_0)^2 + \gamma_{P2W}(R_P/R_0)^2 - \gamma_{P1W} \quad (3)$$

where R_P is the outer radius of the complete particle; R'_P, the radius at the P1P2 interface; R''_P, the radius at the P1P3 interface; and γ_{P1W}, the interfacial tension between polymer 1 and the aqueous phase. Because the interfacial area of the P1P3 interface is independent of the amount of P2 in the particle, (R_P/R_0), (R'_P/R_0), and (R''_P/R_0) can be described only in terms of *volume or weight ratios* of polymers, *not as volume fractions* as was possible for two component particles.[12] As such, eq. (3) becomes

$$(\Delta\gamma)_{CSP3P1P2} = \gamma_{P1P3}(\mathrm{VRP3P1})^{2/3} + \gamma_{P1P2}(\mathrm{VRP3P1} + 1)^{2/3} + \gamma_{P2W}(\mathrm{VRP2P1} + \mathrm{VRP3P1} + 1)^{2/3} - \gamma_{P1W} \quad (4)$$

where VRP3P1 is the volume ratio of P3 to P1 in the final particle, etc. Given the various interfacial tensions, the reduced free energy can be computed for any given choice of polymer ratios. In the limit as P3 goes to zero, eq. (4) simplifies to the two-component core–shell morphology analogy as discussed earlier.[12] The reduced free-energy equations

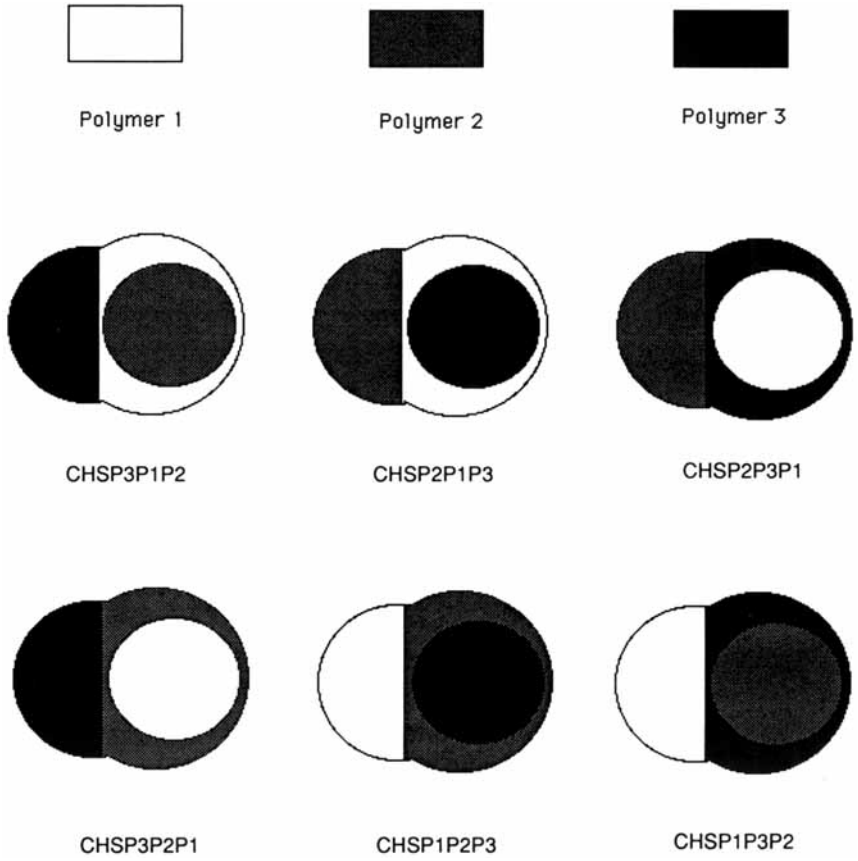

Figure 5 Cored hemisphere morphologies for three-component latex particles.

for all of the other morphologies shown in Figures 1–5 are listed in their final form in the Appendix.

Equation (4) and its companion equations found in the Appendix can be utilized to determine that morphology which possesses the lowest free energy (equivalently the lowest value of $\Delta\gamma$) for any particular experimental system. The only complicating factor in utilizing these equations is having readily available and reliable interfacial tension values. These can be approximated in the absence of experimentally determined values, as will be discussed later.

EXPERIMENTAL

As we have shown previously[12,19] the artificial latex approach is a very simple and useful means to observe morphology development in composite particles. Since the particles are in the 1–10 μm range and a light microscope is used to view the morphology, refractive indices must be relied upon to contrast the phases within the particles. Four polymers, poly(methyl methacrylate) (PMMA, Eastman Kodak Co.), polystyrene (PSty, Aldrich Chemical Co.), poly(dimethyl siloxane) (PDMS, Polysciences, Inc.), and bisphenol-A polycarbonate (PC, Scientific Polymer Products), were chosen to investigate morphology development within three-component emulsion particles, and their physical characteristics are shown in Table I.

The emulsions were made by dissolving three polymers in a mutual solvent (methylene chloride, HPLC grade, J. T. Baker Chemical Co.) at 10 wt % total polymer and dispersing the solution into an aqueous phase using a laboratory homogenizer (Biospec Products Homogenizer). Fifteen grams of the polymer solution were dispersed into 50 g of aqueous phase that contained either sodium lauryl sulfate (SLS, Aldrich Chemical Co.) or a natural pectin (Mexpectin XSS-100 [MXP], Grinsted Products, Denmark) at 0.5 wt % surfactant. The solvent was then removed in two different manners: solvent evaporation from emulsion on a microscope slide and total solvent removal in stirred flask. The former involved placing a drop of freshly made emulsion onto a glass slide and observing the morphology development over time as the solvent evap-

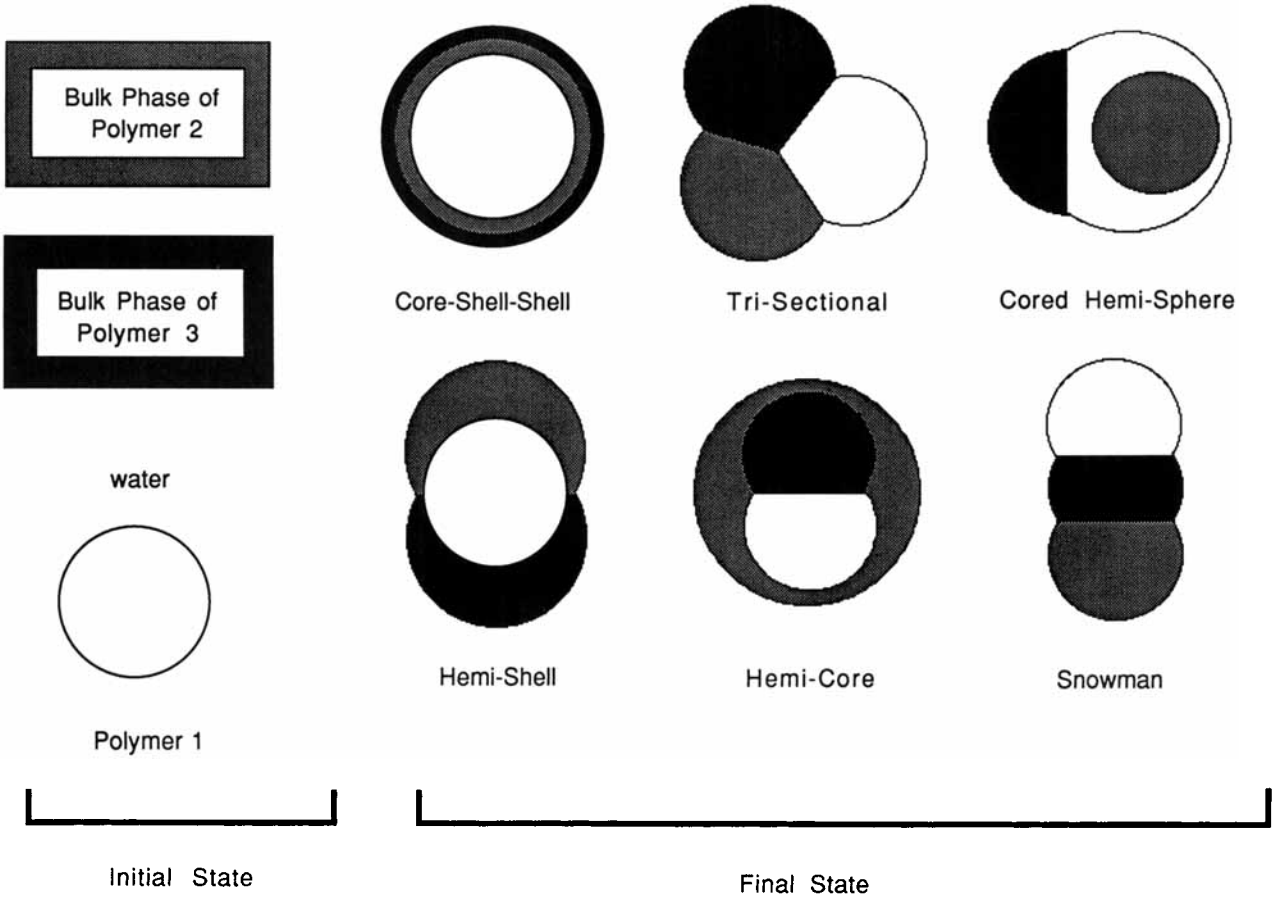

Figure 6 Initial and final states for thermodynamic analysis.

orated to the surrounding atmosphere, while the latter involved stirring the emulsion in an open beaker for at least 15 h to complete solvent removal. Particle morphology was observed in a light microscope (BH-2, Olympus Optical Co.) equipped with a 35 mm camera (OM-4, Olympus Optical Co.) using a Hoffman modulated lens.

The interfacial tensions for various polymers against the two surfactant solutions were determined by contact-angle measurements of an aqueous phase drop on a compression-molded planar polymer surface (for PMMA, PSty, and PC) or by the drop-weight-volume method[22] for the PDMS as it was a viscous liquid. Young's equation

$$\gamma_{pw} = \sigma_p - \sigma_w \cos \theta \qquad (5)$$

where σ_p is the surface tension of the polymer; γ_{pw}, the interfacial tension between the polymer and the surfactant solution; σ_w, the surface tension of the surfactant solution; and θ, the contact angle, was used to calculate the polymer/water interfacial tension for PMMA, PSty, and PC. Table II lists the values of σ_p used for these three polymers. Since the PDMS is a liquid, the drop-weight-volume tensiometer was used to directly determine the PDMS/aqueous interfacial tension. Because of the possible problems

Table I Physical Properties of Polymers

Polymer	Refractive Index[a]	Molecular Weight
PMMA	1.50	102,000[b]
PSty	1.60	83,000[c]
PDMS	1.40	36,000[d]
PC	1.58	64,000[d]

[a] Values taken from Refs. 20 and 21.
[b] Number-average molecular weight as determined by GPC (THF as solvent, ambient temperature, PMMA standards for calibration) in this work.
[c] Number-average molecular weight as determined by GPC (THF as solvent, ambient temperature, PSty standards for calibration) in this work.
[d] Number-average molecular weight as specified by the respective suppliers of these polymers.

in using this method with very viscous liquids, we chose to measure the PDMS/aqueous interfacial tensions for a range of PDMS molecular weights ($\bar{M}_n$ = 340, 770, 3900, 5200) and to interpolate the γ value at $\bar{M}_n$ = 36,000 from plots of the interfacial tensions vs. $(\bar{M}_n)^{-2/3}$ as suggested by LeGrand and Gaines[23] and Wu.[24] A very high molecular weight PDMS gum ($\bar{M}_n > 250{,}000$) was used in a contact-angle experiment to obtain an approximation to the infinite molecular weight point on the γ vs. $(\bar{M}_n)^{-2/3}$ curve so as to provide for an interpolation procedure. The various polymer/aqueous interfacial tensions so determined are listed in Table II.

RESULTS AND DISCUSSION

Eight different three-component systems (four polymer combinations each in aqueous solutions of SLS and MXP) were investigated. These systems included PMMA/PSty/PDMS/SLS(aq); PMMA/PSty/PDMS/MXP(aq); PMMA/PSty/PC/SLS(aq); PMMA/PSty/PC/MXP(aq); PMMA/PDMS/PC/SLS(aq); PMMA/PDMS/PC/MXP(aq); PSty/PDMS/PC/SLS(aq); and PSty/PDMS/PC/MXP(aq). All eight systems were investigated in order to generate a variety of stable morphologies, but only half of the six morphological groups were observed.

To determine interfacial tension values between two polymers, the harmonic mean equation[25]

$$\gamma = \sigma_1 + \sigma_2 - (4\sigma_1^d\sigma_2^d)/(\sigma_1^d + \sigma_2^d) - (4\sigma_1^p\sigma_2^p)/(\sigma_1^p + \sigma_2^p) \quad (6)$$

can be used as an estimation. Here, γ is the interfacial tension; σ_1, the surface tension of polymer 1; σ_2, the surface tension of polymer 2; σ_1^d, the dispersion component of the surface tension of polymer 1; σ_2^d, the dispersion component of the surface tension of polymer 2; σ_1^p, the polar component of the surface tension of polymer 1; and σ_2^p, the polar component of the surface tension of polymer 2. Polymer surface tension and polarity values can be found in the literature and the applicable ones are shown in Table II. The dispersion and polar components sum to the surface tension and the polarity is defined as $x^p = \sigma^p/\sigma$.

Table II Interfacial and Surface Tensions

A. Interfacial Tensions

System	γ (mN/m)	Method
PMMA/SLS (aq)	10.7	Contact angle
PSty/SLS (aq)	13.2	Contact angle
PDMS/SLS (aq)	15.0	Drop-weight-volume
PC/SLS (aq)	11.4	Contact angle
PMMA/MXP (aq)	14.7	Contact angle
PSty/MXP (aq)	28.0	Contact angle
PDMS/MXP (aq)	43.3	Drop-weight-volume
PC/MXP (aq)	21.9	Contact angle
PMMA/PSty	2.0	Estimated by harmonic mean equation[a]
PMMA/PDMS	7.0	Estimated by harmonic mean equation[a]
PMMA/PC	1.0	Estimated by harmonic mean equation[a]
PSty/PDMS	6.0	Estimated by harmonic mean equation[a]
PSty/PC	1.8	Estimated by harmonic mean equation[a]
PDMS/PC	6.5	Estimated by harmonic mean equation[a]

B. Surface Tensions and Polarities

Polymer	Surface tension	Polarity	Reference
PMMA	41.1	0.28	25
PSty	40.7	0.17	25
PDMS	19.8	0.04	25
PC	40.8	0.26	17

[a] See Appendix, Section H.

Table III Computational Results for Three-component Polymer Systems

System	$\Delta\gamma$ (mN/m)				
	1	2	3	4	5
PMMA/PSty/PDMS/SLS	20.2 (SM)	20.3 (STS)	20.3 (CS)	20.4 (CHS)	20.7 (HC)
PMMA/PSty/PDMS/MXP	25.1 (CS)	25.4 (HC)	33.0 (CS)	34.6 (CHS)	36.8 (HS)
PMMA/PSty/PC/SLS	14.2 (HC)	14.4 (HS)	14.5 (CHS)	14.5 (CS)	14.5 (CS)
PMMA/PSty/PC/MXP	19.0 (HC)	19.3 (CS)	20.9 (CS)	24.2 (CHS)	25.5 (HS)
PMMA/PDMS/PC/SLS	18.9 (STS)	19.1 (SM)	19.2 (CS)	19.3 (HS)	19.4 (CHS)
PMMA/PDMS/PC/MXP	24.0 (CS)	24.8 (HC)	29.2 (CHS)	30.4 (HS)	32.1 (CHS)
PSty/PDMS/PC/SLS	18.0 (STS)	18.1 (SM)	18.4 (CHS)	19.0 (SM)	19.1 (HS)
PSty/PDMS/PC/MXP	26.4 (CS)	26.5 (HC)	29.9 (CHS)	30.6 (HS)	32.2 (CHS)

CS, core–shell–shell; HC, hemicore; HS, hemishell; STS, simplified trisectional; SM, snowman; CHS, cored hemisphere.

While the experimental approach begins with all three polymers in solution within the latex particle and Figure 6 shows a different initial state, a few words need to be said about the applicability of eq. (2) (and all subsequent $\Delta\gamma$ equations) to the experiments. The thermodynamic analysis allows us to add solvent to the initial state described in Figure 6 in order to create the initial experimental state. Here, there would be an enthalpy change upon mixing. Then, we allow the single-phase particle to undergo phase separation without solvent loss, followed by solvent removal. Here, the free-energy change involves the negative of the enthalpy change of mixing seen in the previous step and also the interfacial energy change due to the creation of new surfaces. The overall free-energy change is just the difference between the interfacial energies of the final and initial states, as the enthalpies of mixing cancel out. Thus, the experimental process can be envisioned within the thermodynamic pathway shown in Figure 6 and the overall free-energy changes are equivalent.

By using eq. (4) and its companion equations found in part G of the Appendix, a prediction of the morphology of each system at equal polymer volume ratios can be made (i.e., the morphology that gives the lowest $\Delta\gamma$ value). Table III lists the eight systems of interest and some of their respective $\Delta\gamma$ values (rounded off to the first decimal). Since there are 22 different possible morphologies, there are also 22 different $\Delta\gamma$ values for each system. For the sake of clarity and comparison, only the five lowest computed values, with the corresponding morphologies shown in parentheses, are listed.

Using the computed results shown in Table III, the morphology of the PMMA/PSty/PDMS/SLS(aq) system is predicted to be the "snowman" variety; in this case, the PMMA would occupy the central region. However, given that all five $\Delta\gamma$ values listed for this system are within $\pm 1\%$ of one another, it may not be surprising to find any one or a combination of these morphologies in the experimental system. Figure 7 shows the experimental results at partial and complete solvent removal and here there is no doubt that the actual morphology is that of trisectional particles. The $\Delta\gamma$ computations suggest that the trisectional morphology has a total interfacial energy only 0.5% higher than that of the lowest $\Delta\gamma$ value and that this morphology would be the second most likely to be observed. Although some of the particles in Figure 7(b) appear to contain only two phases, they are in reality three-phase, trisectional particles rotated in space as to only show two phases.

Following the same approach, it was predicted that when the surfactant is changed from SLS to MXP for the PMMA/PSty/PDMS system, the morphology should shift to core–shell–shell. The computed $\Delta\gamma$ values listed in Table III show close results for the core–shell–shell and hemicore morphologies, but much higher results for any other morphology. Photos of the experimental morphologies are shown in Figure 8 at partial and complete solvent removal. Here, it is quite clear that the particles are of the hemicore nature. Those at complete solvent removal appear to show one of the interior phases "bursting out" of the shell. Figure 8(b) also shows how well the interior polymer/polymer interface can at times be seen by this simple microscopic technique.

By replacing the very nonpolar PDMS with PC, which has a polarity nearly as high as PMMA, it was found that all five morphologies listed in Table III were predicted to be nearly as likely to be found when SLS was used as a surfactant. The "most likely" morphology for this PMMA/PSty/PC/SLS(aq) system was computed to be hemicore and

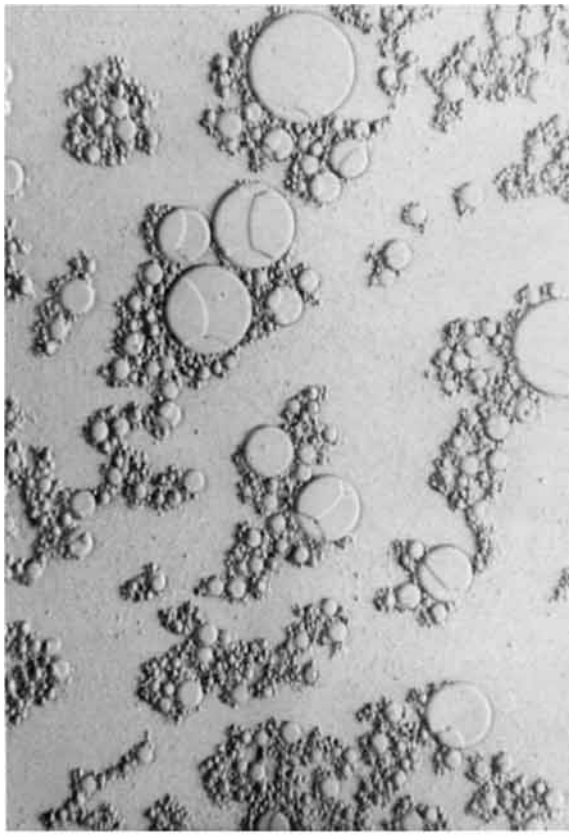

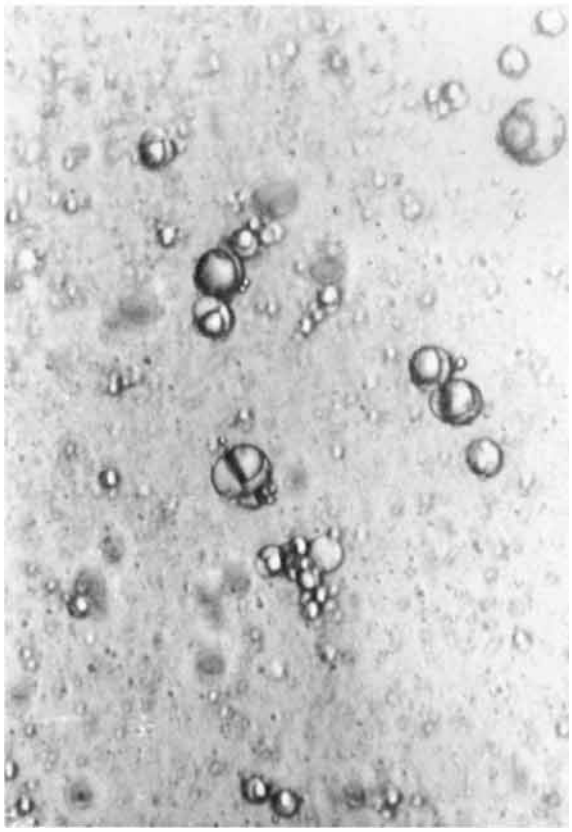

the experimental morphologies shown in Figure 9 show concurrence. At partial solvent removal [Fig. 9(a)], many particles appear to take on some sort of a hemishell or "skewed" hemicore morphology. At total solvent removal, the morphology is more distinctively hemicore. A change of surfactants from SLS to MXP does not change the prediction of the " most likely" morphology, but does lead to greater separation of the other $\Delta\gamma$ values shown in Table III. Figure 10, again at partial and total solvent removal, displays excellent photos of the hemicore morphology. It is of interest here to note that Figure 10(b) does not show any particles with one of the interior phases "bursting out," as seen for the PMMA/PSty/PDMS/MXP(aq) system observed in Figure 8(b).

In the next system of interest, we have chosen to work with two polar polymers and a very nonpolar one. The predicted $\Delta\gamma$ values for the PMMA/PDMS/PC/SLS(aq) system shown in Table III indicate that the trisectional, "snowman," core–shell–shell, hemishell, and cored hemisphere all have very nearly the same probability of existence. The experimental results for this system are shown in Figure 11(a) and 11(b), the latter representing total solvent removal. These photos show clear evidence of the cored hemisphere morphology. Although it is not possible from these photos to tell which polymer envelopes the core, the thermodynamic analysis suggests that the PMMA envelopes the PDMS. A change in surfactants for the PMMA/PDMS/PC system from SLS to MXP causes all the $\Delta\gamma$ values to increase because of the significantly higher polymer/aqueous phase interfacial tensions. The computed results shown in Table III reflect this in that the lowest two energies are associated with those morphologies having a single polymer phase (PMMA in this case) interfacing with the aqueous solution. The other morphological choices display significantly higher $\Delta\gamma$ values. Thus, one would expect to see either the core–shell–shell or the hemicore morphology in this case, with the former being somewhat favored. These photomicrographs of the emulsions made for this PMMA/PDMS/PC/MXP(aq) system are displayed in Figure 12. Here, there is no question that the morphology during and after the solvent removal process is that of hemicore. Figure 12(b) shows one of the interior phases apparently "bursting out" of the shell, as seen in Figure 8(b) for the PMMA/PSty/PDMS/MXP(aq) system.

Figure 7 Photomicrographs of polymer particles for the PMMA/PSty/PDMS/SLS(aq) system at (a) partial and (b) complete solvent removal.

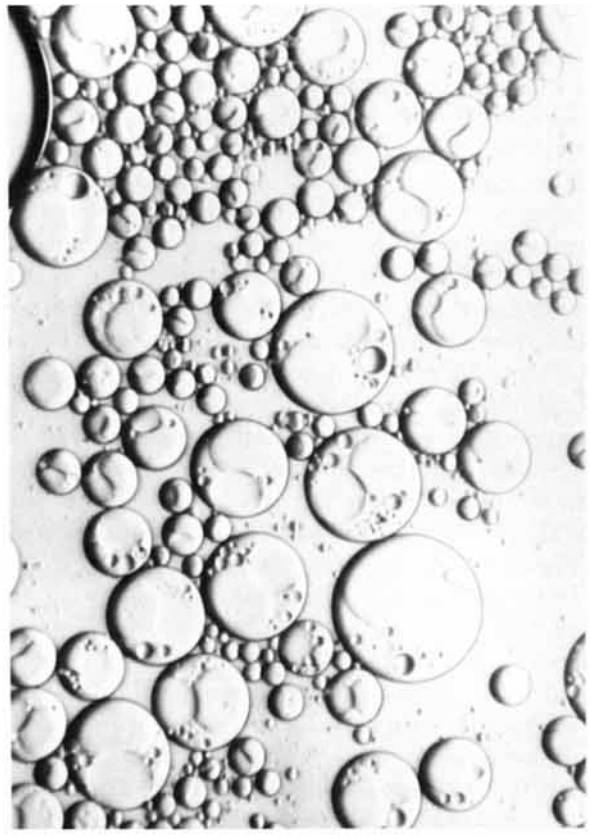

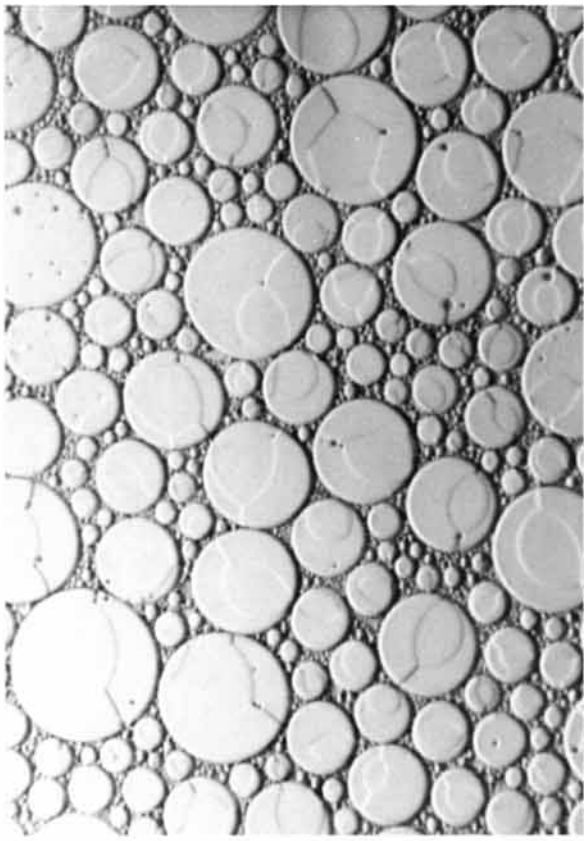

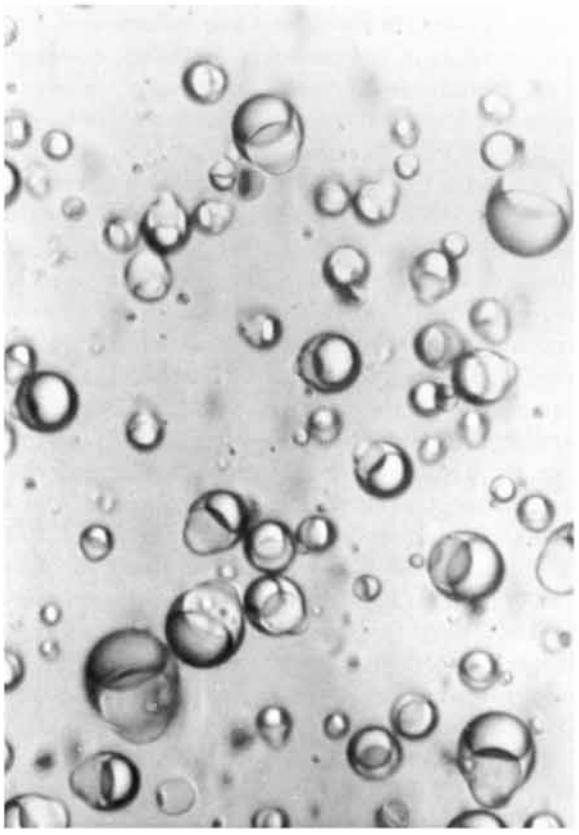

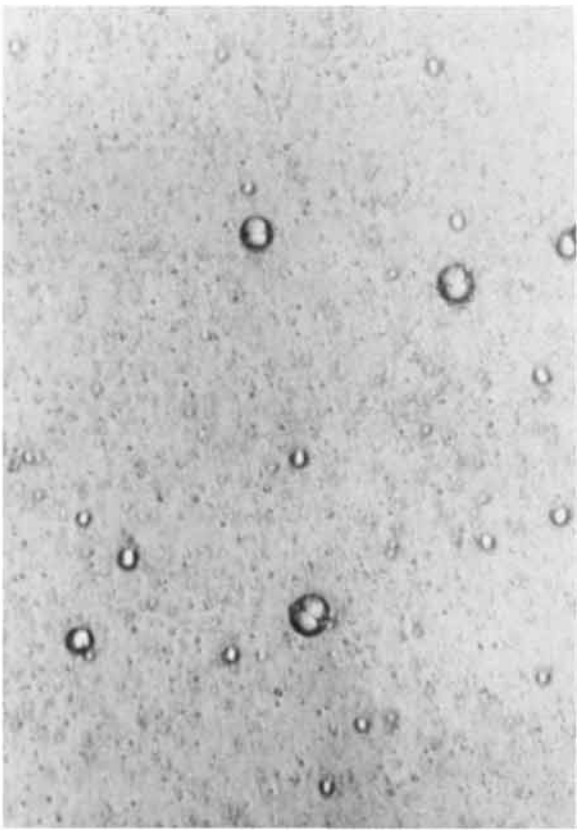

Figure 8 Photomicrographs of polymer particles for the PMMA/PSty/PDMS/MXP(aq) system at (a) partial and (b) complete solvent removal.

Figure 9 Photomicrographs of polymer particles for the PMMA/PSty/PC/SLS(aq) system at (a) partial and (b) complete solvent removal.

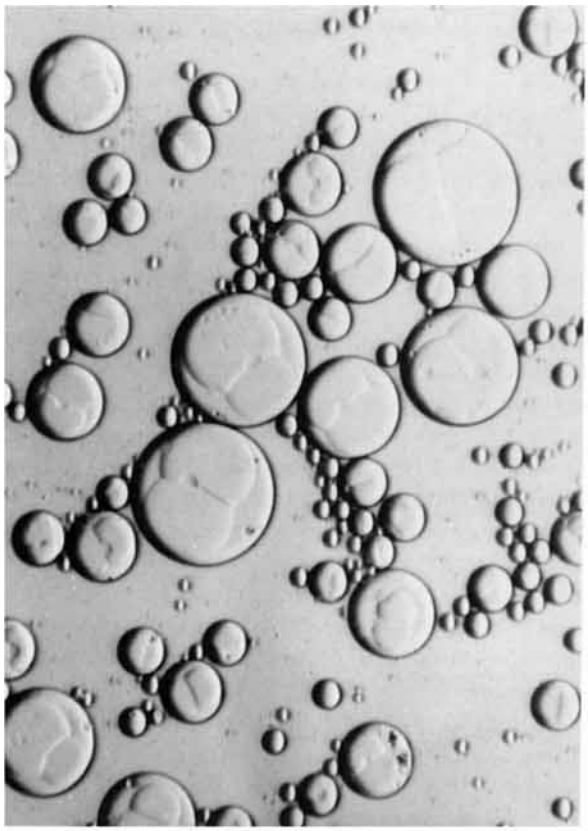

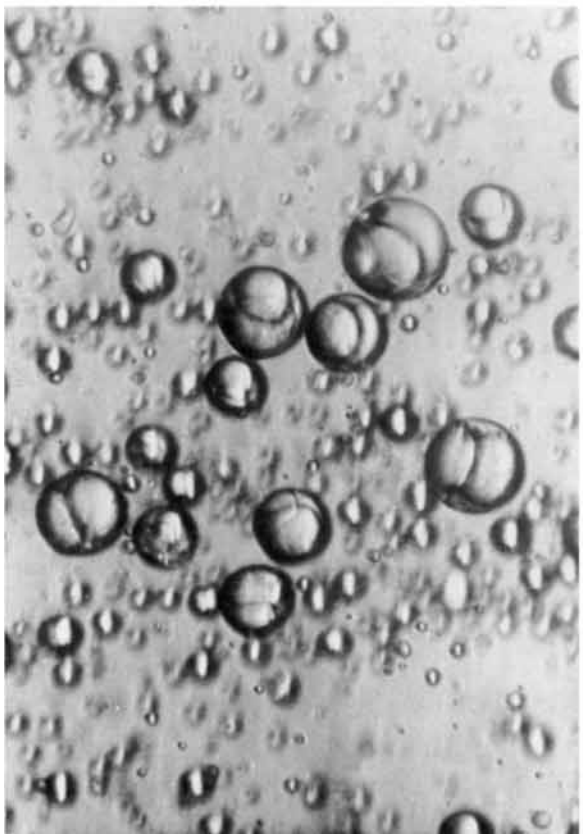

Figure 10 Photomicrographs of polymer particles for the PMMA/PSty/PC/MXP(aq) system at (a) partial and (b) complete solvent removal.

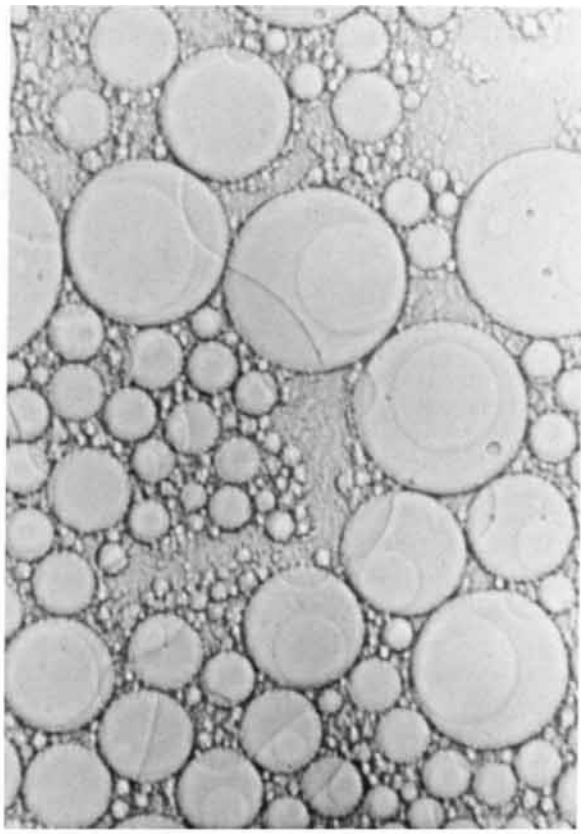

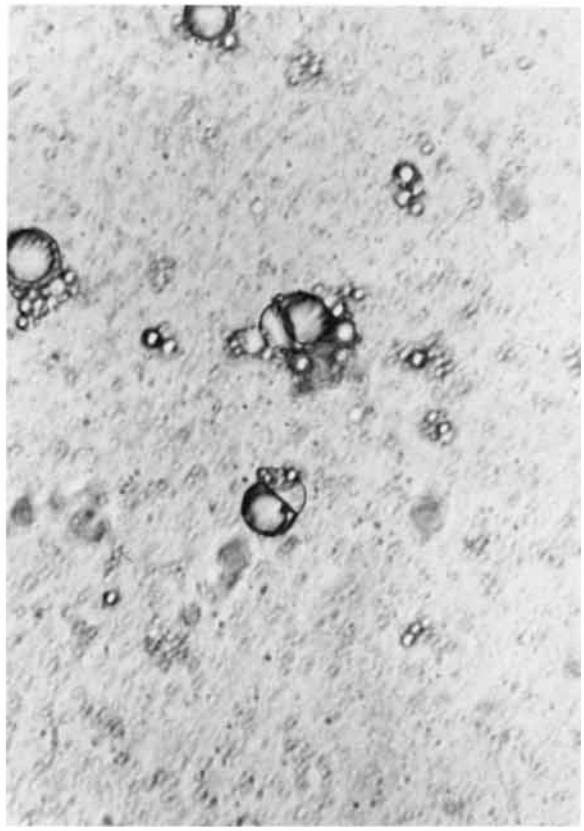

Figure 11 Photomicrographs of polymer particles for the PMMA/PDMS/PC/SLS(aq) system at (a) partial and (b) complete solvent removal.

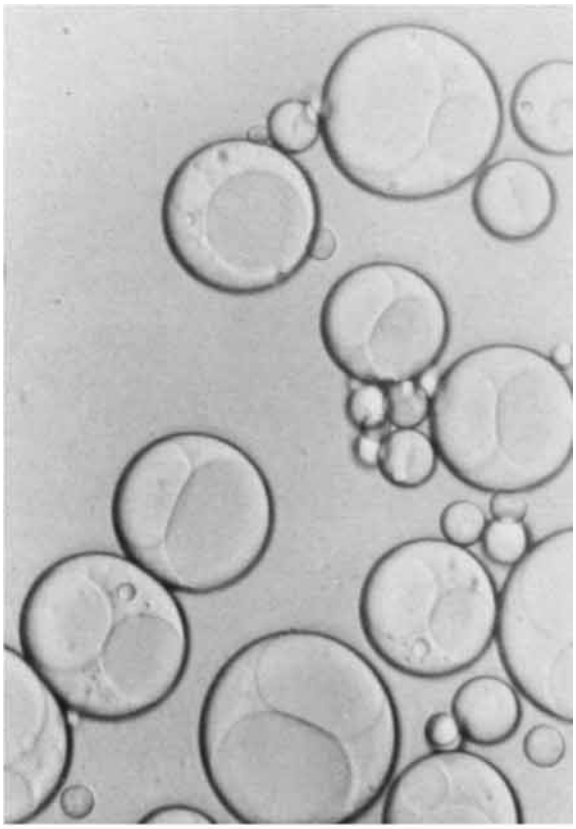

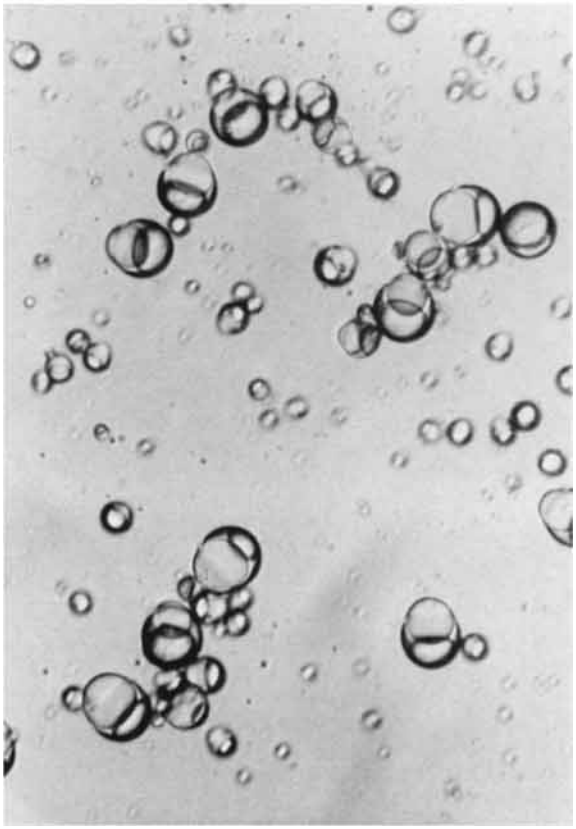

The last system that we worked with is PSty/PDMS/PC. When SLS is used to stabilize the emulsion, the predicted $\Delta\gamma$ values again show very close results for a variety of morphologies, including the "snowman" version. Although the trisectional morphology is computed to be the "most likely" of these, the experiments result in the cored hemispheres shown in Figure 13. It is interesting to note here that the phase contrast between the core and its enveloping phase is much poorer than that in any of the previous micrographs. This diminished phase contrast is particularly troublesome when viewing the PSty/PDMS/PC/MXP(aq) system shown in Figure 14. We are unable to conclude which morphology dominates from these two photos, but a "best guess" on our part would be cored hemispheres as in Figure 13. However, the computations done for this system (Table III) strongly suggest that core–shell–shell or hemicore morphologies are to be expected.

In reviewing all of the above results, it is interesting to note that only three of the six possible morphological families were observed using the polymers and surfactants discussed here. Most surprisingly for us was that the core–shell–shell version was never seen, although in three of eight cases it was computed to be the morphology of choice, and in most of the other cases, it was predicted to have a free-energy value very close to that of the minimum. The reason for this may lie in the approximations used to obtain polymer/polymer interfacial tensions (via the harmonic mean equation and due to the scarcity of published data and difficulty of obtaining experimental data) and some of the geometric simplicities used to generate the $\Delta\gamma$ equations listed in the Appendix. This has not been investigated further at this time. Another point of interest is that changing surfactant characteristics dramatically (SLS lowering polymer/water interfacial tensions markedly and MXP lowering them very little) had mixed effects on the morphology, sometimes changing it and sometimes not. Computationally, the switch from SLS to MXP served to clearly reduce the morphological options, as demonstrated by the values displayed in Table III.

CONCLUDING REMARKS

The extension of the free-energy calculations to three-component particles has been shown to be

Figure 12 Photomicrographs of polymer particles for the PMMA/PDMS/PC/MXP(aq) system at (a) partial and (b) complete solvent removal.

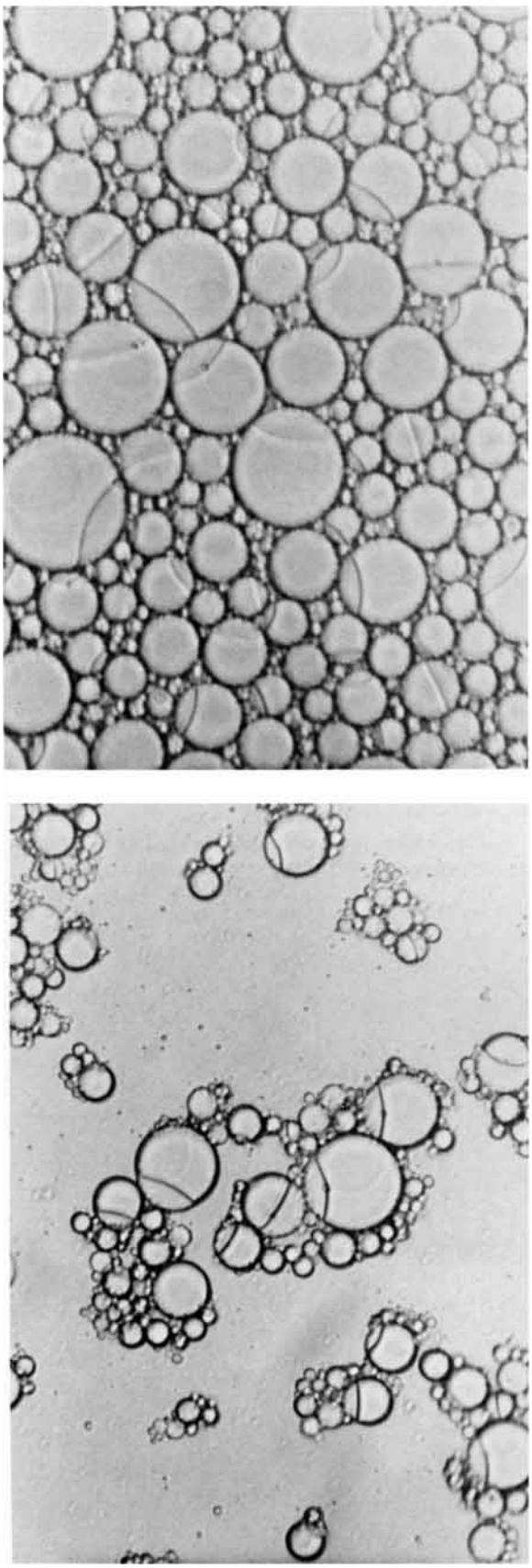

Figure 13 Photomicrographs of polymer particles for the PSty/PDMS/PC/SLS(aq) system at (a) partial and (b) complete solvent removal.

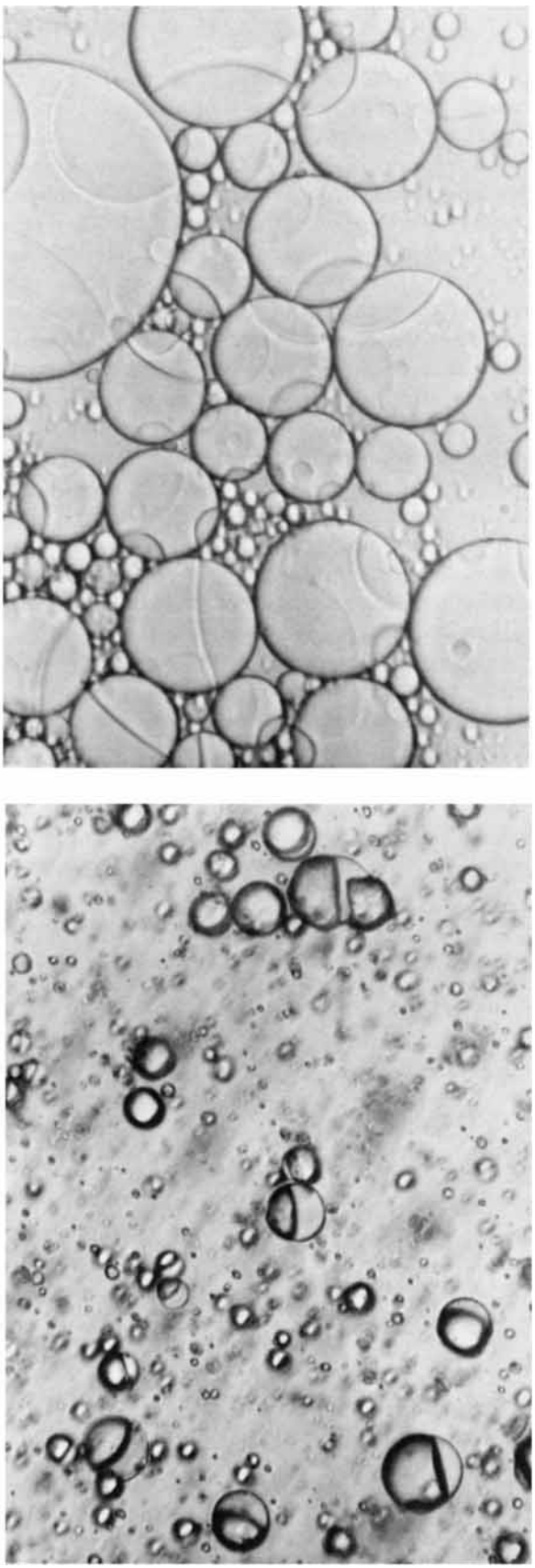

Figure 14 Photomicrographs of polymer particles for the PSty/PDMS/PC/MXP(aq) system at (a) partial and (b) complete solvent removal.

quite straightforward, although tedious due to the large number of morphological alternatives involved. Apparently, there is significant probability that several uniquely different equilibrium morphologies may have very nearly the same free energy and lead to some uncertainties in the ability to clearly predict the particle morphology. This is more likely to happen when very surface active stabilizers (like SLS) are used since they tend to create polymer/water interfacial tensions that are not too different for polymers with significant differences in polarity. This may suggest that more accurate values of all the interfacial tensions are needed to make clear predictions in the three-component systems than in the two-component systems. Nonetheless, the simple thermodynamic analysis described here (even with its sometimes simplified geometric considerations and approximations of polymer/polymer interfacial tensions) has been of great help in anticipating the outcome of experiments.

A final comment may be useful regarding the nature of the experiments reported here. Using the solvent evaporation technique to create artificial latices has allowed us to remove the solvent very gradually from the emulsion particles and likely to approach equilibrium conditions throughout the process. In chemically reactive systems that produce synthetic latices, the dynamic nature of the reaction can lead to situations in which reaction kinetics proceed faster than do phase separation kinetics. This can lead to nonequilibrium, or rate-limited, morphologies that may not be characteristic of the equilibrium particle structure. Our experience in two-component emulsion polymers has shown that such rate limitations often lead to highly occluded structures and such experiments may not yield useful results with which to compare with thermodynamic computations.

We are grateful for the partial financial support provided by the donors of the Petroleum Research Fund of the American Chemical Society and by the University of New Hampshire.

APPENDIX

Parts A–F of this Appendix describe in detail the process by which the surface free-energy equations of one of the morphologies of each basic morphological group is found. Part G lists all 22 surface free-energy equations. Some of these equations are restricted to equal polymer volume ratios of the three components where noted.

A. The interfacial areas applicable to the CSP2P1P3 particle morphology [Fig. A.1(a)] are written as follows:

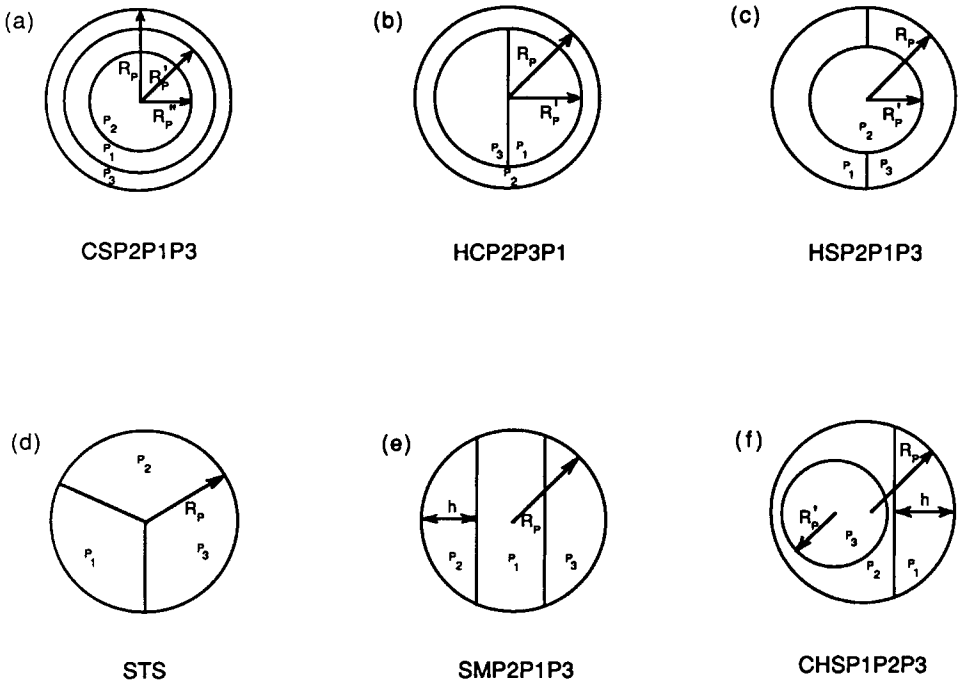

Figure A.1 Dimensional characteristics of the basic morphologies for three-component latex particles.

$$A_{P1P2} = 4\pi(R''_P)^2$$

$$A_{P1P3} = 4\pi(R'_P)^2$$

$$A_{P3W} = 4\pi(R_P)^2$$

Thus, the free-energy change for the particle is

$$(\Delta G)_{CSP2P1P3} = \gamma_{P1P2}[4\pi(R''_P)^2] + \gamma_{P1P3}[4\pi(R'_P)^2] + \gamma_{P3W}[4\pi(R_P)^2] - \gamma_{P1W}[4\pi(R_0)^2] \quad (A.1)$$

Normalizing eq. (A.1) by the surface area of the original particle, $4\pi R_0^2$, and the above volume ratio equations yields

$$(\Delta\gamma)_{CSP2P1P3} = \gamma_{P1P2}(VRP2P1)^{2/3} + \gamma_{P1P2}(VRP2P1 + 1)^{2/3} + \gamma_{P3W}(VRP2P1 + VRP3P1 + 1)^{2/3} - \gamma_{P1W} \quad (A.2)$$

where VRP2P1 = $[4/3\pi(R''_P)^3]/[4/3\pi(R_0)^3] = [4/3\pi(R''_P)^3]/\{4/3\pi[(R'_P)^3 - (R''_P)^3\}$ and VRP3P1 = $\{4/3\pi[(R_P)^3 - (R'_P)^3]\}/[4/3\pi(R_0)^3]$. The calculations for $(\Delta\gamma)_{CSP2P1P3}$, as well as other CS calculations, are exact due to the simple spherical geometry associated with them.

B. The interfacial areas applicable to the HCP2P3P1 particle morphology [Fig. A-1(b)] are written as follows:

$$A_{P1W} = 4\pi(R_P)^2$$

$$A_{P1P2} = 2\pi(R'_P)^2$$

$$A_{P1P3} = 2\pi(R'_P)^2$$

$$A_{P2P3} = \pi(R'_P)^2$$

Thus, the free-energy change for this particle is

$$(\Delta G)_{HCP2P3P1} = \gamma_{P1W}[4\pi(R_P)^2] + \gamma_{P1P2}[2\pi(R'_P)^2] + \gamma_{P1P3}[2\pi(R'_P)^2] + \gamma_{P2P3}[\pi(R'_P)^2] - \gamma_{P1W}[4\pi R_0^2] \quad (A.3)$$

Normalizing eq. (A.3) by the surface area of the original particle, $4\pi R_0^2$, and the above volume ratio equations yields

$$(\Delta\gamma)_{HCP2P3P1} = \gamma_{P1W}[(2VRP2P1 + 1)^{2/3} - 1] + 1/2(2VRP2P1)^{2/3}(\gamma_{P1P2} + \gamma_{P1P3} + 1/2\gamma_{P2P3}) \quad (A.4)$$

where VRP2P1 = $\{1/2[4/3\pi(R'_P)^3]\}/[4/3\pi(R_0)^3] = \{1/2[4/3\pi(R'_P)^3]\}/\{4/3\pi[(R_P)^3 - (R'_P)^3]\}$ Equation (A.3) is found through assuming the simplified geometry illustrated in Figure A.1(b), whereas eq. (A.4) is found through assuming equal polymer volumes. Thus, $(\Delta\gamma)_{HCP2P3P1}$, and other HC calculations, are approximate representations of the actual surface-energy calculations.

C. The interfacial areas applicable to the HSP2P1P3 particle morphology [Fig. A.1(c)] are written as follows:

$$A_{P1P2} = 2\pi(R'_P)^2$$

$$A_{P2P3} = 2\pi(R'_P)^2$$

$$A_{P1P3} = \pi[(R_P)^2 - (R'_P)^2]$$

$$A_{P1W} = 2\pi(R_P)^2$$

$$A_{P2W} = 2\pi(R_P)^2$$

Thus, the free-energy change for this particle is

$$(\Delta G)_{HSP2P1P3} = \gamma_{P1P2}[2\pi(R'_P)^2] + \gamma_{P2P3}[2\pi(R'_P)^2] + \gamma_{P1P3}\{\pi[(R_P)^2 - (R'_P)^2]\} + \gamma_{P1W}[2\pi(R_P)^2] + \gamma_{P2W}[2\pi(R_P)^2] - \gamma_{P1W}(4\pi R_0^2) \quad (A.5)$$

Normalizing eq. (A.5) by the surface area of the original particle, $4\pi R_0^2$, and the above volume ratio equations yields

$$(\Delta\gamma)_{HSP2P1P3} = 1/2(VRP2P1)^{2/3}(\gamma_{P1P2} + \gamma_{P2P3}) + 1/4[(2VRP3P1 + VRP2P1)^{2/3} - (VRP2P1)^{2/3}]\gamma_{P1P3} + 1/2(2VRP3P1 + VRP2P1)^{2/3} \times (\gamma_{P1W} + \gamma_{P2W}) - \gamma_{P1W} \quad (A.6)$$

where VRP2P1 = $[4/3\pi(R'_P)^3]/(4/3\pi R_0^3)$ and VRP3P1 = $(1/2\{4/3\pi[(R_P)^3 - (R'_P)^3]\})/(4/3\pi R_0^3)$. Equation (A.5) is found through assuming the simplified geometry illustrated in Figure A.1(c), whereas eq. (A.6) is found through assuming equal polymer volumes. Thus, $(\Delta\gamma)_{HSP2P1P3}$, as well as other HS calculations, are approximate representations of the actual surface-energy calculations.

D. The interfacial areas applicable to the STS particle morphology [Fig. A.1(d)] are written as follows:

$$A_{P1P2} = 1/2\pi R_P^2$$

$$A_{P1P3} = 1/2\pi R_P^2$$

$$A_{P2P3} = 1/2\pi R_P^2$$

$$A_{P1W} = 4/3\pi R_P^2$$

$$A_{P2W} = 4/3\pi R_P^2$$

$$A_{P3W} = 4/3\pi R_P^2$$

Thus, the free-energy change for this particle is

$$(\Delta G)_{STS} = (\gamma_{P1P2} + \gamma_{P1P3} + \gamma_{P2P3})(1/2\pi R_P^2) + (\gamma_{P1W} + \gamma_{P2W} + \gamma_{P3W}) \times (4/3\pi R_P^2) - \gamma_{P1W}(4\pi R_0^2) \quad (A.7)$$

Normalizing eq. (A.7) by the surface area of the original particle, $4\pi R_0^2$, and the above volume ratio equation yields

$$(\Delta\gamma)_{STS} = (\gamma_{P1P2} + \gamma_{P1P3} + \gamma_{P2P3})(1/8)(3VRP2P1)^{2/3} + (\gamma_{P1W} + \gamma_{P2W} + \gamma_{P3W})(1/3) \times (3VRP2P1)^{2/3} - \gamma_{P1W} \quad (A.8)$$

where $VRP2P1 = [1/3(4/3\pi R_P^3)]/(4/3\pi R_0^3)$.

Equation (A.7) is found through assuming the simplified geometry illustrated in Figure A.1(d), whereas eq. (A.8) is found through assuming equal polymer volumes. Thus, $(\Delta\gamma)_{STS}$ is an approximate representation of the actual surface-energy calculation.

E. The interfacial areas applicable to the SMP2P1P3 particle morphology [Fig. A.1(e)] are written as follows:

$$A_{P1W} = 4\pi R_P^2 - 4\pi R_P h$$
$$A_{P2W} = 2\pi R_P h$$
$$A_{P3W} = 2\pi R_P h$$
$$A_{P1P2} = 2\pi R_P h - \pi h^2$$
$$A_{P1P3} = 2\pi R_P h - \pi h^2$$

Thus, the free-energy change for this particle is

$$(\Delta G)_{SMP2P1P3} = \gamma_{P1W}(4\pi R_P^2 - 4\pi R_P h) + (\gamma_{P2W} + \gamma_{P3W})(2\pi R_P h) + (\gamma_{P1P2} + \gamma_{P1P3}) \times (2\pi R_P h - \pi h^2) - \gamma_{P1W}(4\pi R_0^2) \quad (A.9)$$

where $\phi_{P2} = [1/3\pi h^2(3R_P - h)]/(4/3\pi R_P^3)$ and $h/R_P = 0.7739$ for equal volumes of P1, P2, and P3 (i.e., $\phi_{P2} = 1/3$).

Normalizing eq. (A.9) by the surface area of the original particle, $4\pi R_0^2$, and the above volume fraction equations yields

$$(\Delta\gamma)_{SMP2P1P3} = (2.0801)[\gamma_{P1W}(0.2261) + (\gamma_{P2W} + \gamma_{P3W})(0.3870) + (\gamma_{P1P2} + \gamma_{P1P3})(0.2372)] - \gamma_{P1W} \quad (A.10)$$

Equation (A.9) is found through assuming the simplified geometry illustrated in Figure A.1(e), whereas eq. (A.10) is found through assuming equal polymer volumes. Thus, $(\Delta\gamma)_{SMP2P1P3}$, as well as other SM calculations, are approximate representations of the actual surface-energy calculations.

F. The interfacial areas applicable to the CHSP1P2P3 particle morphology [Fig. A.1(f)] are written as follows:

$$A_{P1W} = 2\pi R_P h$$
$$A_{P2W} = 4\pi R_P^2 - 2\pi R_P h$$
$$A_{P1P2} = 2\pi R_P h - \pi h^2$$
$$A_{P2P3} = 4\pi (R'_P)^2$$

Thus, the free-energy change for this particle is

$$(\Delta G)_{CHSP1P2P3} = \gamma_{P1W}(2\pi R_P h) + \gamma_{P2W}(4\pi R_P^2 - 2\pi R_P h) + \gamma_{P1P2}(2\pi R_P h - \pi h^2) + \gamma_{P2P3}[4\pi (R'_P)^2] - \gamma_{P1W}(4\pi R_0^2) \quad (A.11)$$

where $\phi_{P1} = [1/3\pi h^2(3R_P - h)]/(4/3\pi R_P^3)$ and $h/R_P = 0.7739$ for equal volumes of P1, P2, and P3 (i.e., $\phi_{P1} = 1/3$).

Normalizing eq. (A.11) by the surface area of the original particle, $4\pi R_0^2$, and the above volume fraction equations yields

$$(\Delta\gamma)_{CHSP1P2P3} = (2.0801)[\gamma_{P1W}(0.3870) + \gamma_{P2W}(0.6131) + \gamma_{P1P2}(0.2372)] + \gamma_{P2P3} - \gamma_{P1W} \quad (A.12)$$

Equation (A.11) is found through assuming the simplified geometry illustrated in Figure A.1(f), whereas eq. (A.12) is found through assuming equal polymer volumes. Thus, $(\Delta\gamma)_{CHSP1P2P3}$, as well as other CHS calculations, are approximate representations of the actual surface-energy calculations.

G. Equations for all possible thermodynamically stable three-component morphologies:

$$(\Delta\gamma)_{CSP1P2P3} = \gamma_{P1P2} + \gamma_{P2P3}(VRP2P1 + 1)^{2/3} + \gamma_{P3W}(VRP2P1 + VRP3P1 + 1)^{2/3} - \gamma_{P1W}$$

$$(\Delta\gamma)_{CSP1P3P2} = \gamma_{P1P3} + \gamma_{P2P3}(VRP3P1 + 1)^{2/3} + \gamma_{P2W}(VRP2P1 + VRP3P1 + 1)^{2/3} - \gamma_{P1W}$$

$$(\Delta\gamma)_{CSP2P1P3} = \gamma_{P2P1}(VRP2P1)^{2/3} + \gamma_{P1P3}(VRP2P1 + 1)^{2/3} + \gamma_{P3W}(VRP2P1 + VRP3P1 + 1)^{2/3} - \gamma_{P1W}$$

$$(\Delta\gamma)_{CSP2P3P1} = \gamma_{P2P3}(VRP2P1)^{2/3} + \gamma_{P1P3}(VRP2P1 + VRP3P1)^{2/3} + \gamma_{P1W}[(VRP2P1 + VRP3P1 + 1)^{2/3} - 1]$$

$$(\Delta\gamma)_{CSP3P1P2} = \gamma_{P1P3}(VRP3P1)^{2/3} + \gamma_{P1P2}(VRP3P1 + 1)^{2/3} + \gamma_{P2W}(VRP2P1 + VRP3P1 + 1)^{2/3} - \gamma_{P1W}$$

$$(\Delta\gamma)_{CSP3P2P1} = \gamma_{P2P3}(VRP3P1)^{2/3} + \gamma_{P1P2}(VRP2P1 + VRP3P1)^{2/3} + \gamma_{P1W}[(VRP2P1 + VRP3P1 + 1)^{2/3} - 1]$$

The following hemicore equations were found by assuming simplified geometry and equal volumes of the three polymer components:

$$(\Delta\gamma)_{HCP2P3P1} = \gamma_{P1W}[(2VRP2P1 + 1)^{2/3} - 1] + 1/2(2VRP2P1)^{2/3}(\gamma_{P1P2} + \gamma_{P1P3} + 1/2\gamma_{P2P3})$$

$$(\Delta\gamma)_{HCP1P2P3} = 1/2(2VRP2P1)^{2/3}(\gamma_{P1P3} + \gamma_{P2P3} + 1/2\gamma_{P1P2}) + \gamma_{P3W}(2VRP2P1 + VRP3P1)^{2/3} - \gamma_{P1W}$$

$$(\Delta\gamma)_{HCP1P3P2} = 1/2(2VRP2P1)^{2/3}(\gamma_{P1P2} + \gamma_{P2P3} + 1/2\gamma_{P1P3}) + \gamma_{P2W}(2VRP3P1 + VRP2P1)^{2/3} - \gamma_{P1W}$$

The following hemishell equations were found by assuming simplified geometry and equal volumes of the three polymer components:

$$(\Delta\gamma)_{HSP1P2P3} = 1/2(\gamma_{P1P2} + \gamma_{P1P3}) + 1/2(2VRP2P1 + 1)^{2/3}(\gamma_{P2W} + \gamma_{P3W}) + 1/4[(2VRP2P1 + 1)^{2/3} - 1] - \gamma_{P1W}$$

$$(\Delta\gamma)_{HSP2P1P3} = 1/2(VRP2P1)^{2/3}(\gamma_{P1P2} + \gamma_{P2P3}) + 1/4 \times [(2VRP3P1 + VRP2P1) - (VRP2P1)^{2/3}]\gamma_{P1P3} + 1/2(2VRP3P1 + VRP2P1)^{2/3} \times (\gamma_{P1W} + \gamma_{P3W}) - \gamma_{P1W}$$

$$(\Delta\gamma)_{HSP3P1P2} = 1/2(VRP3P1)^{2/3}(\gamma_{P1P3} + \gamma_{P2P3}) + 1/4 \times [(2VRP2P1 + VRP3P1) - (VRP3P1)^{2/3}]\gamma_{P1P2} + 1/2(2VRP2P1 + VRP3P1)^{2/3} \times (\gamma_{P1W} + \gamma_{P2W}) - \gamma_{P1W}$$

The following simplified trisectional equation was found by assuming simplified geometry and equal volumes of the three polymer components:

$$(\Delta\gamma)_{STS} = 1/3(\gamma_{P1W} + \gamma_{P2W} + \gamma_{P3W})(3VRP2P1)^{2/3} + 1/8(\gamma_{P1P2} + \gamma_{P2P3} + \gamma_{P1P3})(3VRP2P1)^{2/3} - \gamma_{P1W}$$

The following snowman equations were found by assuming simplified geometry and equal volumes of the three polymer components:

$$(\Delta\gamma)_{SMP2P1P3} = (2.0801)[\gamma_{P1W}(0.2261) + (\gamma_{P2W} + \gamma_{P3W})(0.3870) + (\gamma_{P1P2} + \gamma_{P1P3})(0.2372)] - \gamma_{P1W}$$

$$(\Delta\gamma)_{SMP1P2P3} = (2.0801)[\gamma_{P2W}(0.2261) + (\gamma_{P1W} + \gamma_{P3W})(0.3870) + (\gamma_{P1P2} + \gamma_{P2P3})(0.2372)] - \gamma_{P1W}$$

$$(\Delta\gamma)_{SMP1P3P2} = (2.0801)[\gamma_{P3W}(0.2261) + (\gamma_{P1W} + \gamma_{P2W})(0.3870) + (\gamma_{P1P3} + \gamma_{P2P3})(0.2372)] - \gamma_{P1W}$$

The following cored hemisphere equations were found by assuming simplified geometry and equal volumes of the three polymer components:

$$(\Delta\gamma)_{CHSP2P3P1} = (2.0801)[\gamma_{P2W}(0.3870) + (\gamma_{P3W}) \times (0.6131) + (\gamma_{P2P3})(0.2372)] + \gamma_{P1P3} - \gamma_{P1W}$$

$$(\Delta\gamma)_{CHSP1P2P3} = (2.0801)[\gamma_{P1W}(0.3870) + (\gamma_{P2W}) \times (0.6131) + (\gamma_{P1P2})(0.2372)] + \gamma_{P2P3} - \gamma_{P1W}$$

$$(\Delta\gamma)_{CHSP1P3P2} = (2.0801)[\gamma_{P1W}(0.3870) + (\gamma_{P3W}) \times (0.6131) + (\gamma_{P1P3})(0.2372)] + \gamma_{P2P3} - \gamma_{P1W}$$

$$(\Delta\gamma)_{CHSP3P1P2} = (2.0801)[\gamma_{P3W}(0.3870) + (\gamma_{P1W}) \times (0.6131) + (\gamma_{P1P3})(0.2372)] + \gamma_{P1P2} - \gamma_{P1W}$$

$$(\Delta\gamma)_{CHSP3P2P1} = (2.0801)[\gamma_{P3W}(0.3870) + (\gamma_{P2W}) \times (0.6131) + (\gamma_{P2P3})(0.2372)] + \gamma_{P1P2} - \gamma_{P1W}$$

$$(\Delta\gamma)_{CHSP2P1P3} = (2.0801)[\gamma_{P2W}(0.3870) + (\gamma_{P1W}) \times (0.6131) + (\gamma_{P1P2})(0.2372)] + \gamma_{P1P3} - \gamma_{P1W}$$

H. Polymer/polymer interfacial tension values can be estimated by the use of eq. (6). Although the surface tension and polarity values referenced in Section B of Table II were directly used in eq. (6), the resulting interfacial tensions were difficult to accept as computed (values as low as 0.1 and as high as 12). This was perhaps due to our need to have consistency among these values for the six polymer pairs that we chose to work with and the fact that the surface tension and polarity values cited in the literature are not necessarily precise quantities themselves. Thus, we made many computations based on minor changes to σ_P and x^P for the four polymers and eventually settled upon the polymer/polymer interfacial tension values shown in Table II. Although we deem these to be reasonable estimates of the values for these polymer pairs and judge them to show consistency with respect to polarity differences, we do not contend that they are precise values. Experimental values of these interfacial tensions would be preferable, but they are not available in the literature to our knowledge. We have previously[18] used $\gamma_{PMMA/PSty} = 1.8$ nM/m at 60°C and, for the purposes of the present work at room temperature, have adjusted the value upward to 2.0 mN/m. Using this as a reference point and eq. (6) as a guide, we set the other γ values as indicated.

REFERENCES

1. D. I. Lee, ACS Symposium Series 165, American Chemical Society, Washington, DC, 1981, p. 405.

2. M. Okubo, Y. Katsuta, and T. Matsumoto, *J. Polym. Sci. Polym. Letter Ed.*, **20,** 45 (1982).
3. D. I. Lee and T. Ishikawa, *J. Polym. Sci. Polym. Chem. Ed.*, **21,** 147 (1983).
4. T. I. Min et al., *J. Polym. Sci. Polym. Chem. Ed.*, **21,** 2845 (1983).
5. S. Muroi, H. Hashimoto, and K. Hosoi, *J. Polym. Sci. Polym. Chem. Ed.*, **22,** 1365 (1984).
6. D. R. Stutman, A. Klein, M. S. El-Aasser, and J. W. Vanderhoff, *Ind. Eng. Chem. Prod. Dev.*, **24,** 404 (1985).
7. I. Cho and K. W. Lee, *J. Appl. Polym. Sci.*, **30,** 1903 (1985).
8. D. J. Hourston, R. Satgurunthan, and H. Varman, *J. Appl. Polym. Sci.*, **31,** 1955 (1986).
9. J. Berg, D. Sundberg, and B. Kronberg, *Polym. Mater. Sci. Eng.*, **54,** 367 (1986).
10. J. Berg, D. Sundberg, and B. Kronberg, *J. Microencap.*, **6,** 327 (1989).
11. S. Lee and A. Rudin, *Makromol. Chem. Rap. Commun.*, **10,** 655 (1989).
12. D. C. Sundberg et al., *J. Appl. Polym. Sci.*, **41,** 1425 (1990).
13. M. Okubo, *Makromol. Chem. Macromol. Symp.*, **35/36,** 307 (1990).
14. M. R. Muscato and D. C. Sundberg, *J. Polym. Sci. Part B Polym. Phys. Ed.*, **29,** 1021 (1991).
15. J.-E. L. Jonsson, H. Hassander, L. H. Jansson, and B. Tornell, *Macromolecules,* **24,** 126 (1991).
16. Y.-C. Chen, V. Dimonie, and M. S. El-Aasser, *J. Appl. Polym. Sci.*, **42,** 1049 (1991).
17. S. Y. Hobbs, M. E. J. Dekkers, and V. H. Watkins, *Polymer,* **29,** 1598 (1988).
18. C. L. Winzor and D. C. Sundberg, *Polymer,* **33,** 3797 (1992).
19. C. L. Winzor and D. C. Sundberg, *Polymer,* to appear.
20. J. Brandrup and E. H. Immergut, *Polymer Handbook,* 3rd ed., Wiley, New York, 1989, pp. 455–457.
21. J. Brandrup and E. H. Immergut, *Polymer Handbook,* 2nd ed., Wiley, New York, 1975, pp. 242.
22. J. L. Lando and H. T. Oakley, *J. Coll. Interface Sci.*, **25,** 526 (1967).
23. D. G. LeGrand and G. L. Gaines, *J. Coll. Interface Sci.*, **31,** 162 (1969); **42,** 181 (1973).
24. S. Wu, in *Polymer Blends,* D. R. Paul and S. Newman, Eds., Academic Press, New York, 1978, Vol. 1, pp. 243–293.
25. S. Wu, *Polymer Interface and Adhesion,* Marcel Dekker, New York, 1982, Chap. 3.

Received February 3, 1992
Accepted April 30, 1992